Nanoscale

Accepted Manuscript

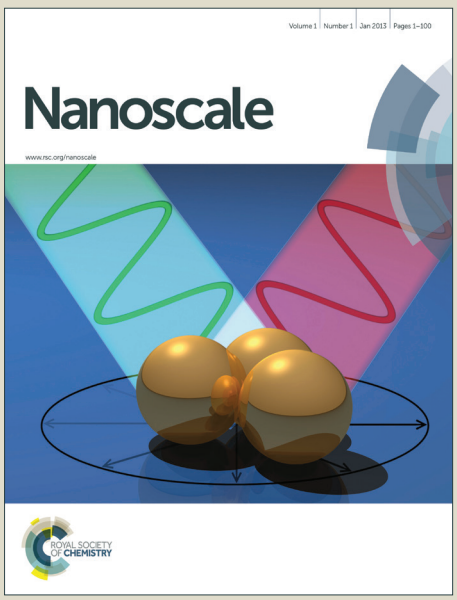

ROYAL SOCIETY OF CHEMISTRY

www.rsc.org/nanoscale

Self-assembly and characterization of Transferrin-gold nanoconstructs and their interaction with bio-interfaces

Birgitte H. McDonagh*[†, ¶], Sondre Volden[†, ¶], Sina M. Lystvet[†], Gurvinder Singh [†], Marit-Helen G. Ese[‡], Joseph A. Ryan[§], Mikael Lindgren[‖], Axel Sandvig[‡,¥], Ioanna Sandvig[‡], Wilhelm R. Glomm[†, p, *]

[†]Ugelstad Laboratory, Department of Chemical Engineering, Norwegian University of Science and Technology (NTNU), 7491 Trondheim, Norway

[‡]SINTEF Energy Research, P.O. Box 4761 Sluppen, N-7465 Trondheim, Norway,

[§]Department of Chemistry, Iona College, New Rochelle, New York, USA

[‖] Department of Physics, Norwegian University of Science and Technology (NTNU), N-7491 Trondheim, Norway.

[‡]Department of Circulation and Medical Imaging, Faculty of Medicine, Norwegian University of Science and Technology, Trondheim, Norway

[¥]Department of Pharmacology and Clinical Neurosciences, Umeå University, 901 87 Umeå, Sweden

[p] Sector for Biotechnology and Nanomedicine, SINTEF Materials and Chemistry, Trondheim, Norway

* Tel: +47-73 55 03 25, fax: +47-73 59 40 80, e-mail: birgitte.h.mcdonagh@ntnu.no,

[¶]These authors contributed equally to this work

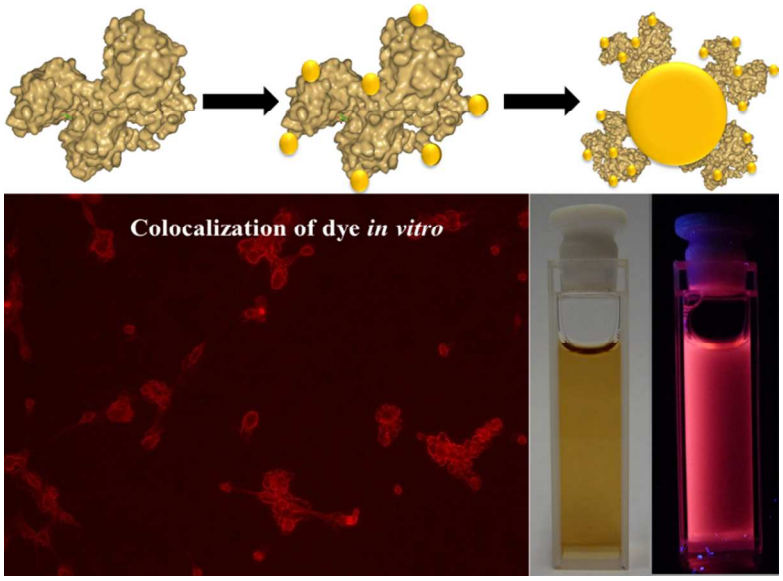

Keywords: Gold nanoclusters, Fluorescence, protein-lipid interaction, atomic force microscopy, Langmuir monolayers, Glioblastoma astrocytoma, Ovarian cancer cells, Olfactory ensheating cells.

ABSTRACT: Transferrin (Tf) conjugated to gold nanoparticles-and clusters combine the protein's site-specific receptor targeting capabilities with the optical properties imparted by the nano-sized gold. We describe two different synthesis protocols, one yielding fluorescent Tf-stabilized gold nanoclusters (AuNCs) and one yielding Tf-stabilized gold nanoparticles that exhibit localized surface plasmon resonance. We demonstrate that the synthetic route employed has a large influence both on the gold nanostructure formed, and also on the structural integrity of the protein. A slight protein unfolding allows stronger interaction with lipids, and was found to significantly perturb lipid monolayers. Interactions between the protein-gold nanostructures and three different cell types were also assessed, indicating that enhanced membrane affinity may be attributed to intercellular membrane differences.

Introduction: The optical properties of nanosized gold are size-dependent. The small gold nanoclusters (AuNCs) range from a few, to tens of atoms and exhibit size-dependent molecular fluorescence. At 3 nm and above, the nanosized gold becomes plasmonic nanoparticles that absorb light in the visible region of the electromagnetic spectrum[1,2] AuNCs and AuNPs can be synthesized via a biomineralized synthesis using proteins, resulting in AuNCs and AuNPs stabilized in a protein template. This class of hybrid nanomaterials has potential applications in bioimaging,[3-8] targeted drug delivery[4,5,8] and sensing.[9-12]

Synthesis of protein-AuNCs constructs is typically achieved via incubation of a protein solution with tetrachloroauric acid (TCAA) either in the presence of a reducing agent such as ascorbic acid[5,6,13,14] or sodium borohydride ($NaBH_4$),[15,16] or by utilizing the Intrinsic redox potential of amino acid residues in the polypeptide chain such as tyrosine and histidine.[3,4,8-12,15,17] Irrespective of the synthesis procedure, growth of protein-AuNCs has been revealed to be protein-mediated as well as highly protein-dependent.[16,17]

While much emphasis has been put on the properties and applications of the embedded metal nanoclusters, little has been reported on the effect of AuNCs incorporation on the structure and properties of the protein scaffold. Recently, we reported that functionalizing proteins with AuNCs results in tunable, protein-dependent changes in structure and function of the polypeptide scaffold.[16,17] Moreover, we have demonstrated that combining proteins and gold on the nanoscale might results in emergent properties (*i.e.;* properties not characteristic of either protein or gold) such as enhanced membrane-affecting properties[15,18,19] and even anticancer activity.[15]

Transferrin (Tf) is a multi-tasking iron-binding protein which has been much researched for active drug delivery due to its efficient site-specific targeting of receptors over-expressed on cancer cell surfaces.[20-22] See e.g. McCann[20] and references therein for a review of the clinical applications of Tf. The ability for Tf to successfully target its specific receptor has been observed while conjugated to to drug carrier systems such as quantum dots,[23] liposomes[24] and gold nanoparticles.[25] Recently, Schneider and coworkers reported that Tf-stabilized AuNCs display similar targeting and cellular uptake characteristics as the native protein. Here, we have used iron-free transferrin as a scaffold for AuNCs synthesis via two synthetic routes; one relying solely on the reduction potential of the protein, and one wherein an extrinsic reducing agent ($NaBH_4$) was added (these protocols are hereafter referred to as Intrinsic and Extrinsic, respectively). For the Tf-AuNCs constructs presented here, we have characterized the photophysical properties, the effect on Tf structure, how incorporation of AuNCs results in enhanced membrane-affecting properties compared to the native protein, and the concomitant effect on cell membrane interaction.

Materials and Methods:

Preparation of Tf-AuNCs

Intrinsic protocol. Apo-transferrin (Sigma) was dissolved in MQ-water to a total concentration of 10mg/mL. Tf-AuNCs were made by adding 1:1 (v/v) of tetrachloroauric acid (5mM, TCAA, Sigma) before adjusting the pH to above 10 (250 µL, 1M NaOH). As a reference, Tf (10mg/mL) was mixed 1:1 (v/v) with MQ-water and pH adjusted as described. The samples were left to react for one week at 37°C. In order to remove excess TCAA, samples were dialysed against deionized (MilliQ) water for two hours, before water exchange and dialysis over night. Samples prepared for cell viability studies were dialysed as described, but against phosphate buffer (pH=7.4). Samples prepared using the Intrinsic protocol is named *Tf-AuINT*. The phosphate buffer was prepared by mixing dipotassium hydrogen phosphate (KH_2PO_4, 50mM, Merck) and potassium dihydrogen phosphate (K_2HPO_4, 50mM, Merck) to a final pH of 7.4[15].

Extrinsic protocol. Samples were prepared and dialysed as described for the Intrinsic protocol, but in addition, an extrinsic reducing agent ($NaBH_4$, 200µL, 1M) was added immediately after TCAA. The same Tf stock solution as described for the Intrinsic protocol was used. The reference was prepared as for the Intrinsic protocol, except that 200µL $NaBH_4$ (1M) was added in addition. This sample was named *Tf-RED*. Two different concentrations of TCAA were used in order to form AuNCs and AuNPs. For Tf-AuNCs, a low concentration of TCAA (1mM) was added 1:1 (v/v) to the Tf-stock solution before adding 200 µL $NaBH_4$. These samples were named *Tf-AuXL*. For extrinsic synthesis of Tf-AuNPs, the same concentration of TCAA as Tf-AuINT was used (5mM), with the addition of 200µL $NaBH_4$ (1M). These samples were named *Tf-AuXH*.

Scanning Transmisison Electron Microscopy (STEM). Hitachi S-5500 electron microscopy operating at 30 kV accelerating voltage was used to record TEM images. Prior to TEM imaging, samples were prepared by placing a few microliters of Tf-AuNCs solution on a TEM grid, before drying and imaging.

High resolution transmission electron microscopy (HR-TEM) images were acquired on a JEOL JEM-2100 (200 kV). The samples were prepared by depositing a few µl drop of nanoparticles or nanoclusters solution on a copper grid coated with amorphous carbon layer, and allowed to dry prior to imaging.

UV-visible Spectroscopy. UV-visible spectroscopy was perfomed on a Shimadzu UV-2401PC spectrophotometer using the *UVprobe 2.10 software.* The Tf-concentration was 10µM.

Steady-state Fluorescence Spectroscopy. Steady-state fluorescence was measured on a Fluorolog-3 HORIBA Jobin Yvon apparatus, using excitation wavelengths λ_{ex} = 295, 370 nm. The Tf concentration was 3.6 µM, and all samples were measured in triplicates.

Time Correlated Single Photon Counting (TCSPC). For TCSPC, an IBH TCSPC spectrometer was employed. The prompt was recorded by setting the emission monochromator at the same wavelength as the light source (λ_{em} = 280 nm). For lifetime measurement of the samples, the emission monochromator was set to λ_{em}=360 nm, with a band-pass of 8 nm for both prompt and samples.

Circular Dichroism (CD). Circular dichroism (CD) was measured on an Olis DSM 1000CD apparatus, equipped with a lamp power supply LPS-220B from Photon Technology International. The user interface was an Olis online instrument system, and the software was OLIS GlobalWorks. For CD measurements, the scan range was set from 290 to 200 nm, with 720 increments. The Tf concentration was 2.3 µM, and the cuvette path length was 10 mm. The grid was 2400 lines/mm, and the slit width was 6.32 mm. Each sample was scanned three times, using the phosphate buffer as blank.

Langmuir Film Experiments. A KSV Langmuir

Minitrough double barrier system (KSV LTD, Finland) was used and the experiments were controlled through the manufacturer's own software. The Langmuir was equipped with a Teflon trough (250mL) and Delrin barriers. The surface pressure probe was made of paper (pre-soaked in the buffer media). Prior to all of the experiments, any surface impurities were removed with a Pasteur pipette connected to a vacuum pump. The AuNCs samples prepared using the Extrinsic protocol were not stable in aqueous solutions and was determined to be unfit for Langmuir film experiments. However, samples of Tf and Tf-AuINT (1 mL, 12.5 μM) had greater stability in solution and were found adequate for Langmuir film experiments. The interfacial activity of the air/buffer surface for each Tf-gold construct was studied by filling the trough (250 mL) with phosphate buffer, closing the barriers to 90 mm, and zeroing the balance. The sample was then injected underneath the lipid surface, from outside of the barriers using a syringe with a ~90° needle.[26] The barriers were kept in constant position, and the surface pressure was recorded over time. For lipid interaction studies, PBPS (60 μL, 0.25 mg/mL dissolved in $CHCl_3$) was compressed with barrier speed 5 mm/min until it reached a surface pressure of 10 mN/m. The system was set to have a constant surface pressure of 10mN/m before Tf or Tf-AuINT was injected as described above. The required surface area was then measured as function of time.

Langmuir-Schaefer Deposition. Gold-covered glass plates were prepared for film deposition by immersion in Piranha solution (H_2SO_4:H_2O_2, 3:1)[27] for 20 minutes before flushing with deionized (MilliQ) water and drying with pressured air. The Tf and Tf-AuINT samples (1 mL, 12.5 μM) were injected as described above, under a lipid film of PBPS. The protein-lipid mixture was left to equilibrate for one hour before the Langmuir−Schaefer deposition was made. The gold-sputtered glass plate was introduced horizontally towards the lipid/air surface, using a vacuum pump to hold the plate. The gold-covered plate was kept at the surface for 30 seconds before it was lifted back up again. The adsorbed layer was then dried in air, and imaged with AFM.

Atomic Force Microscopy (AFM). ScanAsyst mode AFM images were acquired by Multimode atomic force microscopy (Nanoscope V controller), Digital Instrument at room temperature. AFM tips with spring constant ~0.4 N/m were purchased from Bruker AFM probes. Samples were prepared as described by Langmuir-Schaefer deposition.

Cell viability studies. Low passage rat olfactory ensheathing cells (OECs, P=6), human glioblastoma-astrocytoma cells (U-87 MG, P>8) and ovarian cancer cells (OCCs, TOV112D) were expanded in six well plates (Costar® 3335, Corning CellBIND® surface, Corning Inc., NY, USA) at 37°C, with 7% and 5% CO_2, respectively, until 70% confluence.

OEC culture. OECs purified from neonatal Fischer rats at P7, were seeded on poly-L-lysine-treated multi-well plates (Costar® 3335, Corning CellBIND® surface, Corning Inc., NY, USA) at a density of 1 x 10^4 cells/cm^2. The cultures were fed with Dulbecco's Modified Eagles Medium (DMEM) GlutaMAX® (Sigma) with 1.25% gentamicin (Sigma) and 5% fetal bovine serum (Autogen Bioclear, Wiltshire, UK) supplemented with 41.6% SATO, 2.7% fibroblast growth factor (FGF, Peprotech), 0.27% heregulin (hrgβ1, R&D Systems Europe Ltd, Abingdon, UK) and 0.05% forskolin (Sigma).

Glioblastoma-astrocytoma culture. Human glioblastoma-astrocytoma cells (U-87 MG, ECACC, Salisbury, UK) were cultured in Eagle's Minimal Essential Medium (EMEM) with 1.25% gentamicin (Sigma) and 10% fetal bovine serum (Autogen Bioclear, Wiltshire, UK). The cultures were supplemented with 2mM L-Glutamine, 1% non-essential amino acids (NEAA, Sigma), and 1mM sodium pyruvate (NaP, Sigma).

OCC culture. Human ovarian cancer cells (OCCs, CRL-11731, ATCC, USA) were cultured in a 1:1 (v/v) solution of Medium 199 (Invitrogen) and Medium 105 (Invitrogen) with 15% fetal bovine serum (Autogen Bioclear, Wiltshire, UK).

Cell labeling with Tf-AuNCs and Tf. Cells at 70% confluency were labeled with Tf and Tf-AuINT at concentrations of nanoparticles/media volume of 1μg/mL, 100μg/mL, 1mg/mL, and incubated at 37°C for 4 hours. Unlabeled OEC, OCC and glioblastoma-astrocytoma cultures, at the same stage of confluence, were used as controls.

LIVE/DEAD® Assay. A LIVE/DEAD-cell viability assay (Invitrogen, Life Technologies) evaluates the membrane integrity of cells, and consists of two different dyes: calcein AM (excitation/emission: 494/517nm) and ethidium homodimer-1 (excitation/emission: 517/617nm). In live cells, intracellular esterases react with calcein AM and yield a cytoplasmic green fluorescence. Ethidium homodimer-1 (EthD-1) diffuses over damaged cell membranes of dead cells, were it binds to nucleic acids and emit red fluorescence. After labeling with Tf-AuINT and Tf, LIVE/DEAD-cell viability was performed on OECs, glioblastoma-astrocytoma cells and OCCs as described by the manufacturer, with one exception. Instead of adding both dyes in one solution, two separate solutions of EthD-1 (12μL EthD-1) in PBS (Sigma, 4.5mL), and calcein (2.7μL) in PBS (Sigma, 4.5mL) were prepared for visualization of dead and live cells, respectively. The reason for this was based on observations of spectral interactions between the fluorescent dyes and the Tf-AuNCs. Three parallels of each cell culture were assayed with either calcein or EthD-1 solutions in 1:1 (v/v), and left to react for 30 min at 37° C before imaging. Imaging of LIVE/DEAD-cell viability assay was performed on an Axiovert 200M fluorescent microscope (Zeiss, Germany), at 40x or 10x magnifications, using AxioVision Rel. 4.3 software. Images were later processed with ImageJ 1.46.

Results and discussion:

The results are grouped into the following categories: photophysical properties of the Tf-AuNCs, effect of incorporation of AuNCs on Tf structure, interaction with lipid monolayers, and cellular interaction studies.

Photophysical properties of the Tf-AuNCs constructs:

Synthesis of protein-stabilized gold can yield several gold species that coexist in or around the protein backbone. In samples where only AuNCs are present, the AuNCs can be detected with fluorescence spectroscopy. When the availability of gold precursor is high or when an extrinsic reducing agent is added, growth of larger AuNPs can occur wherein AuNC-stabilized proteins self-assemble around gold nanoparticles exhibiting localized surface plasmon resonance (LSPR).[16] When AuNPs and AuNCs are in close proximity, the AuNPs can quench the emitted fluorescence from AuNCs.[28]

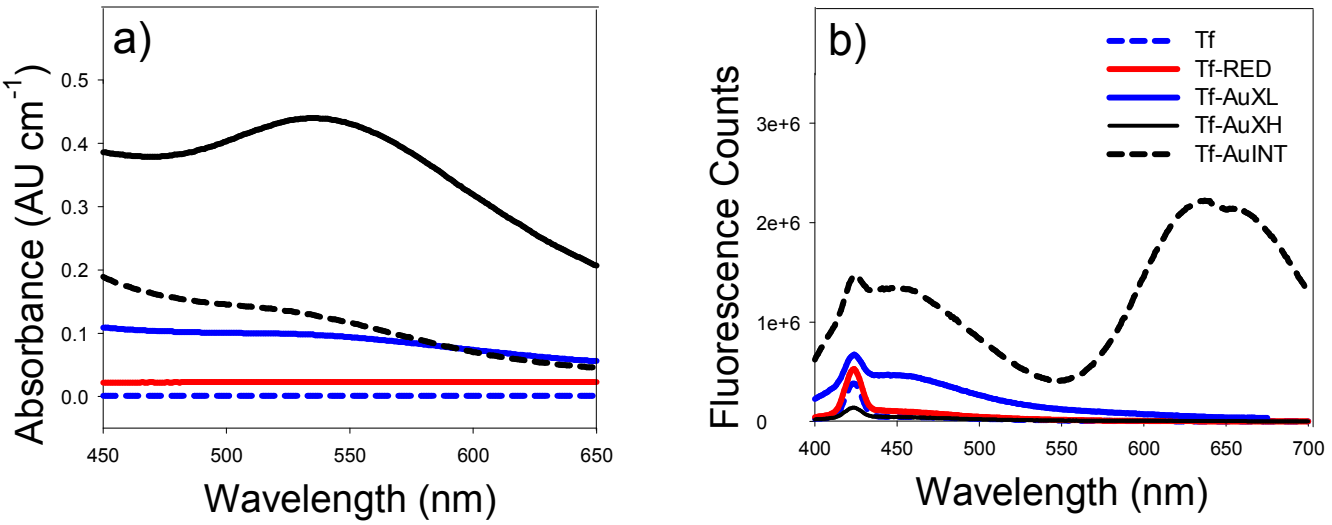

Figure 1a) UV-Visble spectra showing LSPR for AuNPs synthesized with a high (Tf-AuXH) and low concentration of TCAA (Tf-AuXL) and AuNPs synthesized via the Intrinsic protocol (Tf-AuINT). All samples were compared to the pure protein (Tf) and Tf with added $NaBH_4$ (Tf-RED). b) Tf-AuNCs emission was measured with excitation λ_{ex}= 370nm.

Excitation (λ_{ex})	Emission (λ_{em})	Specie
λ_{ex}= 370 nm	λ_{em}= 450 nm	AuNCs(Au_8)
λ_{ex}= 370 nm	λ_{em}= 650 nm	AuNCs(Au_{25+})
λ_{ex}= 295 nm	λ_{em}= 350 nm	Tryptophan in Tf
λ_{ex}= 278 nm	λ_{em}= 350 nm	Tryptophan and tyrosine in Tf

Table 1: Overview of excitation and emission wavelengths used in steady-state fluorescence spectroscopy and TCSPC.

Thus, in a sample with predominantly AuNPs, fluorescence emission of AuNCs is quenched, while the UV-visible absorbance of plasmonic AuNPs increase.

UV-visible spectra of the different Tf-AuNCs studied here, as well as the reference systems (Tf only and Tf treated with $NaBH_4$), are shown in Figure 1a. While the spectral line shape was found to vary both with respect to synthetic route and concentration of TCAA, all the Tf-stabilized nano gold systems displayed a broad absorption band from ~450-600 nm, compared to the protein alone. This is an indication of multimeric gold species.[15-17] While the LSPR feature is prominent in the Tf-AuXH system, the band observed for Tf-AuINT has lower absorbance and occur at shorter wavelengths, indicating smaller AuNPs. The larger AuNPs synthesized via the Extrinsic route is thus most likely a result of the added extrinsic reducing agent ($NaBH_4$).

The fluorescence profile of protein-templated AuNCs upon excitation at ~370 nm is typically assigned to contributions from gold nanoclusters containing 8 atoms (Au_8 , λ_{em} ~450 nm) and gold nanoclusters with 25 atoms (Au_{25} , λ_{em} ~650 nm).[3,5,7,9,11,13] In order not to overstate the accuracy of our obtained results, we have opted to classify the AuNCs as either "small" (~Au_8, λ_{em} ~450 nm) or "large" (Au_{25+}, $\lambda_{em} \geq 600$ nm).[15-17] Steady-state emission spectra of the Tf-AuNCs upon excitation at 370 nm are shown in Figure 1b. Emission spectra from Tf and Tf treated with $NaBH_4$ (Tf-RED) are shown as reference. From the emission spectra shown in Figure 1b, the fluorescence line shape of the Tf-AuNCs varies both with respect to synthetic route and the concentration of TCAA added. The Tf-AuNCs obtained using the Extrinsic synthesis route (Tf-AuXL and Tf-AuXH), the lowest concentration of TCAA (Tf-AuXL) resulted in modest fluorescence emission at ~450 nm, indicating the presence of small AuNCs (Au_8), whereas no fluorescence at this wavelength could be detected for the higher TCAA concentration (Tf-AuXH). From the spectra acquired for Tf-AuXL, the concentration of gold precursor (TCAA) will have an effect on the size of the AuNCs. We attribute the absence of emission at 450 nm for Tf-AuXH to efficient quenching from AuNPs that are in close proximity to the AuNCs (see Figure 1a for the UV-visible spectrum of the potential energy acceptor). Synthesis of Tf-AuNCs via the Intrinsic synthesis route resulted in Tf-AuNCs with vastly improved fluorescence intensity, as seen from the Tf-AuINT spectrum in Figure 1b. In addition to the contribution from small AuNCs emission at ~450 nm, the fluorescence of the Tf-AuINT is dominated by emission above 600 nm. Exact determination of the number of gold atoms associated with each emitting protein-embedded AuNCs population is very complex, and the emission attributed to the larger AuNCs often comprises at least two contributions. This can be observed from the bimodal peak at 650nm in Figure 1b.

Because of the complex interactions between fluorescent AuNCs and colloidal gold, HRTEM can be used as complementary to UV-visible and steady-state fluorescence spectroscopy. Indeed, for the intrinsic protocol (Tf-AuINT, Figure 2a-b) both AuNPs and AuNCs were found. A larger population of AuNPs were found for Tf-AuXH, while no AuNPs were found for Tf-AuXL. The only difference between Tf-AuINT and Tf-AuXH is the addition of $NaBH_4$ in the latter. From UV-visible, steady-state fluorescence spectra and HRTEM images, the addition of $NaBH_4$ clearly increase the amount of AuNPs in the sample. Although AuNPs are also present in the intrinsic samples, it is ultimately the concentration of AuNPs that will determine the amount of AuNC quenching. Tf-AuINT has a dominant near-infrared (NIR) fluorescence together with weak LSPR (Figure 1a), indicating that the concentration of AuNPs is less compared to Tf-AuXH.

In order to further investigate the photophysical properties of the Tf-stabilized AuNCs, time-resolved fluorescence data was collected at λ_{em} = 650 nm using time-resolved single photon counting (TCSPC) spectroscopy with an excitation wavelength of λ_{ex} = 373 nm. The steady-state emission (Figure 1b) of Tf-AuXL is very low at 450 nm and is completely absent for Tf-AuXH. Because of this, no lifetimes could be obtained for these samples. However, time-resolved fluorescence data Tf-AuINT (λ_{em} = 650 nm) were collected, and fitted with a biphasic decay.

The fractional contribution of each decay time to the steady-state intensity, *f,* can be determined from the decay times, *τ,* and *α* which is the relative population of the components at *t* = 0, and is shown in equation 1[28].

$$f_i = \frac{\alpha_i \tau_i}{\sum_j \alpha_j \tau_j} \qquad (1)$$

All the Tf systems studied here were best fit by biphasic decay, yielding one short (τ_1) and one long (τ_2) lifetime and their relative populations α_1 and α_2.[28] Lifetimes of 0.49 ns and 1.78 ns, with corresponding populations 33.7% and 66.3% were determined for Tf-AuINT. Peak broadening and bimodal fluorescence at ~650nm with steady-state fluorescence emission (Figure 1b) combined with two observable lifetimes at 650 nm, could reveal the presence of at least two different-sized AuNCs.

Effect of AuNCs formation on Transferrin structure

Tryptophan (Trp) emission is a well-documented spectroscopic method for studying conformational changes such as partial unfolding in proteins.[28] Unfolding changes the local environment of Trp residues, and depending on the number and location of the Trp residues, this might lead to changes in fluorescence line shape, with respect to both emission maximum and intensity. While changes in fluorescence intensity alone can be difficult to interpret, shifts in the emission maximum towards longer wavelengths are generally linked to protein unfolding.[15-19,28] Trp emission spectra (λ_{ex} = 295 nm) of the systems studied here are shown in Figure 3a. For the Tf-AuNCs synthesized by the Extrinsic route, it is apparent that $NaBH_4$ affects the local environment of Trp residues, leading to a reduction of Trp emission intensity compared to that of the native protein. While the exact effect of $NaBH_4$ on Tf conformation cannot be elucidated from the Trp fluorescence alone, the spectra in Figure 3a reveal that synthesis of Tf-AuNCs via the Extrinsic protocol employed here leads to changes in Trp emission not attributable to the reducing agent alone, but is strongly dependent on TCAA concentration. Specifically, a low concentration of TCAA resulted in a red-shift as well as a severe attenuation of Trp fluorescence (Tf-AuXL). Increasing the TCAA concentration while at the same time adding $NaBH_4$ resulted in complete quenching of Trp emission (Tf-AuXH). Within this sample, large AuNPs were formed, which implies that the larger the gold species, the greater the change in protein conformation.

Using a biomineralization-inspired synthesis protocol (no $NaBH_4$, Tf-AuINT) a red-shift and broadening of the fluorescence line shape and an overall attenuation of the signal was observed. Albeit not as severe as was found for Tf-AuXL, the partial unfolding of the polypeptide chain is attributed to incorporation of large AuNCs.

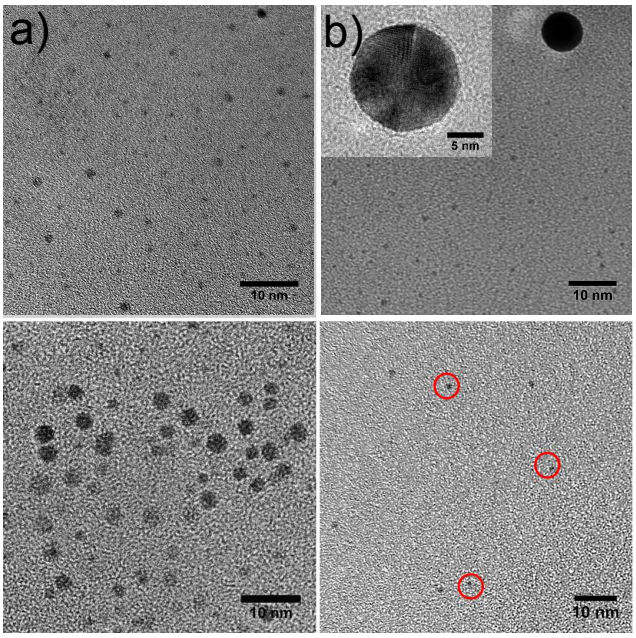

Figure 2 a) HR-TEM image of AuNCs prepared via the Intrinsic protocol. b) Co-existance of AuNPs and AuNCs synthesized via the intrinsic protocol. The inset show an Tf-stabilized AuNP synthesized from the Tf only. Image c) show HRTEM images of AuNCs and AuNPs synthesized via the extrinsic protocol, with high and d) low amount of TCAA added. The red circles indicate AuNCs.

The effect of AuNCs formation on the Trp environment was also studied using TCSPC using λ_{ex} = 278 nm, with the results summarized in Table 2. As for the Tf-AuINT, the time-resolved fluorescence data was best fit with biphasic decay (equation 1). In addition, the average lifetime,$\bar{\tau}$, was calculated as shown in equation 2[28]:

$$\bar{\tau} = \frac{\alpha_1\tau_1^2+\alpha_2\tau_2^2}{\alpha_1\tau_1+\alpha_2\tau_2} = f_1\tau_1 + f_2\tau_2 \qquad (2)$$

It should be noted that in using an excitation wavelength of 278 nm, the collected signal also contains minor contributions from other aromatic amino acid residues such as tyrosine in addition to Trp fluorescence[28]. From the results shown in Table 2, neither the lifetimes nor the associated populations are significantly affected by the addition of $NaBH_4$. No lifetimes could be obtained for the Tf-AuXH sample, which is in agreement with the complete quenching observed from steady-state fluorescence (Figure 3a). For the Tf-AuXL system, there is a minor decrease in the average lifetime compared to the native protein. This is attributed to a decrease in Trp lifetimes, in particularly τ_1, whereas the associated populations remained relatively unchanged. We attribute this to quenching from increased solvent exposure due to partial unfolding, energy transfer (FRET) to the embedded AuNCs, or a combination of these effects.[15,16] The biggest change in the average lifetime was calculated for Tf-AuINT. This indicates larger changes in the local environment of Trp compared to native Tf.

TCSPC (λ_{ex} =278nm, λ_{em} =360nm)						CD
	τ_1 (ns)	τ_2 (ns)	α_1 (%)	α_2 (%)	$\bar{\tau}$ (ns)	I200/I222
Tf	1.45	3.52	55	45	2.8	1.7
Tf-Red	1.47	3.62	56	44	2.9	1.8
Tf-AuXL	0.64	3.11	54	46	2.6	2.7
Tf-AuINT	1.06	4.03	36	64	3.6	4.0

Table 2: TCSPC data for Tf, Tf-RED and Tf-AuNCs emission (λ_{ex} = 278 nm, λ_{em} = 360 nm) and CD data. Tf refer to pure transferrin, while Tf-RED is Tf with added $NaBH_4$. Tf-AuXL were prepared with adding a low concentration of TCAA (Extrinsic protocol), while Tf-AuINT were synthesized via the Intrinsic protocol. τ_1 and τ_2 is the short and long lifetime, respectively, while the α_1 and α_2 is the corresponding population. $\bar{\tau}$ is the average lifetime calculated from the relative populations and their respective lifetimes. The CD measurement is a ratio of of the mean residual ellipticity at 200 and 222nm.

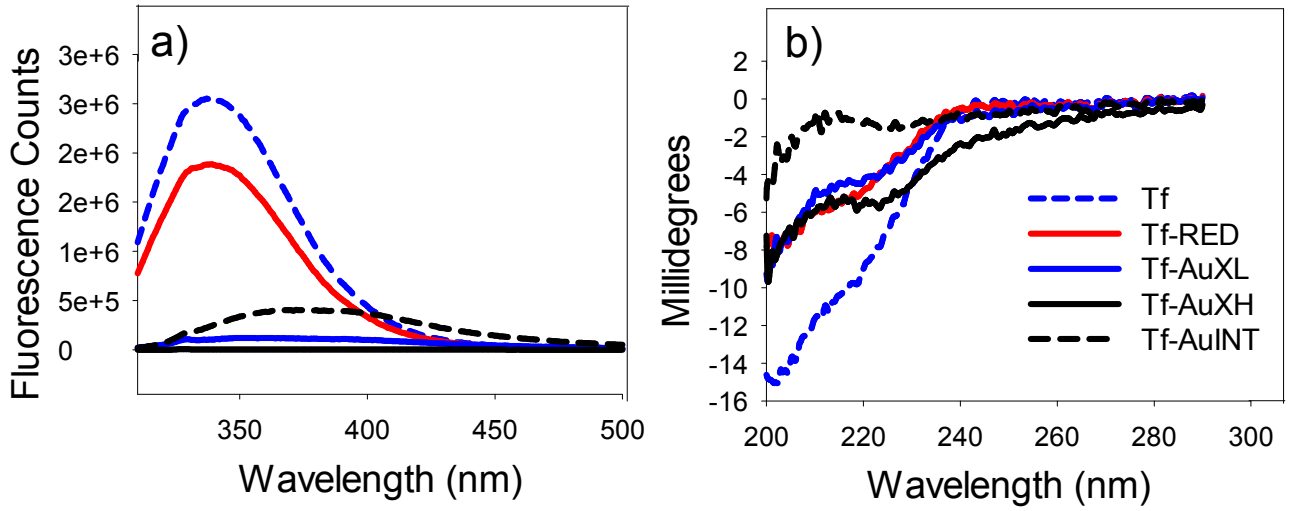

Figure 3 a) Trp emission of native Tf (Tf) has the highest fluorescence intensity at 350nm when excited at λ_{ex}=295nm compared to Tf with $NaBH_4$ (Tf-RED), Tf-AuNCs prepared with no (Tf-AuINT), high (Tf-AuXH) and low (Tf-AuXL) concentration of TCAA. When a high concentration of TCAA is used, the Trp emission is almost completely quenched (Tf-AuXL). b) CD traces indicate structural changes in the protein backbone as the line shape changes when compared to the native protein (Tf), both with respect to $NaBH_4$ and TCAA.

Specifically, both the population and lifetime of τ_2 increases relative to Tf only, whereas the opposite is seen for τ_1. The complex structure of the Tf-AuINT system with both AuNCs of different sizes in each protein, with multiple poteins assembled around a central AuNP core (9.42±0.16 nm) makes the interpretation of the TCSPC results with respect to effect on protein structure qualitative at best.

In order to better elucidate the effect of AuNCs incorporation on protein structure, circular dichroism (CD) measurements were performed on the systems studied here. The CD spectra shown in Figure 3b reveal that Tf secondary structure is significantly affected by both incorporation of AuNCs and by the reducing agent used in the Extrinsic protocol. These findings are consistent with what we have reported earlier.[15,16] In order to ascertain that the observed changes in CD profiles did not emanate from signal attenuation from scattering contribution or reduction in protein concentration due to aggregation and subsequent precipitation, changes in the CD line shape were estimated via the ratio of mean residual ellipticity at 200 nm and 222 nm (I200/I222, Table 2). A reduction of protein concentration or signal attenuation due to scattering from gold species is expected to result in a signal reduction without affecting the line shape. However, since the line shape varies between the species studied here as shown in Table 2, it is likely that the changes in CD profile compared to Tf only are due to structural changes in the protein, which is also in agreement with steady-state and time-resolved Trp fluorescence results.

Interaction with lipid monolayers

We have previously demonstrated that modification of proteins with gold nanoparticles and –clusters can significantly alter lipid interaction compared to the native protein.[15,18,19]

The change in surface pressure upon injecting Tf and Tf-AuINT under an air/water interface (phosphate buffer, pH 7.4) is shown in Figure 4a. The AuNCs samples prepared using the Extrinsic protocol were not found to be sufficiently stable for

the Langmuir experiments. Consequently, only Tf and Tf-AuINT results are shown here. Injecting Tf only into the PBPS lipid layer, did not yield any measurable changes in surface pressure even after an hour, indicating that the native protein has negligible surface activity under these conditions. On the other hand, injection of Tf-AuINT resulted in a rapid and significant surface pressure increase, revealing that modification with AuNCs results in increased surface activity of the protein. This is likely due to increased exposure of hydrophobic residues in the protein following AuNCs formation, which is in agreement with fluorescence and CD results presented above, as well as earlier studies.[15-19]

The average changes in trough area upon injection of Tf and Tf-AuINT under a precompressed phospholipid film are shown in Figure 4b. The lipid used here, porcine phosphatidylserine (PBPS), is negatively charged and is partly dissolved (~20%) during the experimental time frame used here (60 minutes at 10 mN/m). Thus, the traces shown in Figure 4b are corrected for phospholipid drift by normalizing with respect to

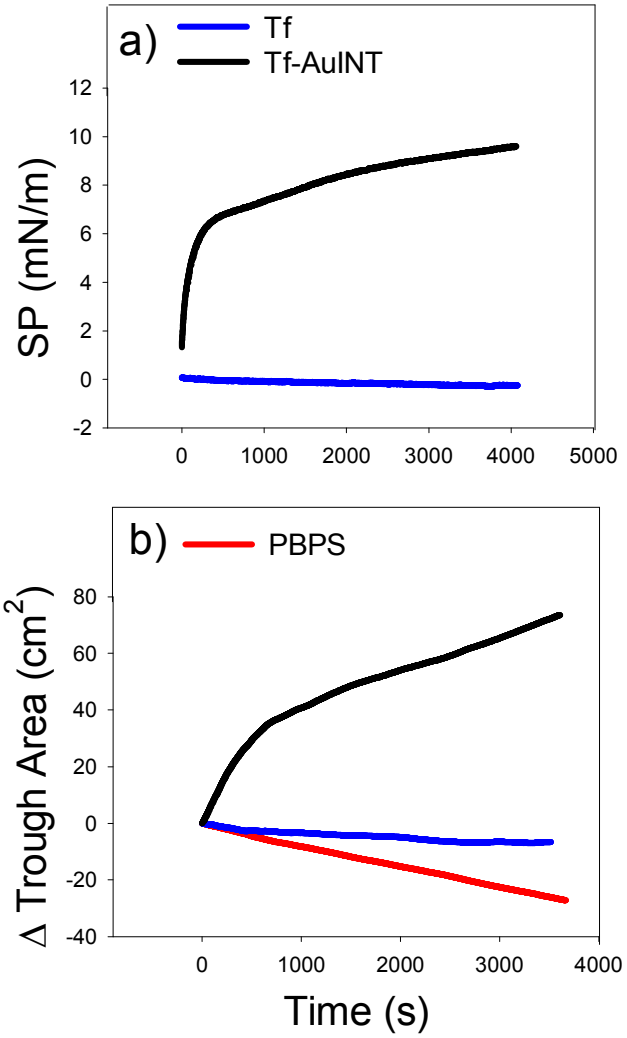

Figure 4 a) Surface pressure as a function of time show that compared to the native protein (Tf), the Tf-AuNCs prepared via the Intrinsic protocol (AuINT) is surface active. b) The delta surface area as a function of time indicates that TfAuINT has a higher surface activity compared to the pure lipid (PBPS) and the native protein (Tf).

the time-dependent surface area behavior of PBPS only. When using the injection method to investigate protein-lipid interactions in a Langmuir trough, the reproducibility is strongly dependent on the injection rate as well as the injection depth, i.e.; distance between the tip of the needle and the lipid monolayer.[29] In particular, the experiment must be discarded if the needle penetrates the lipid film, or if air bubbles are injected into the subphase and disturbing the monolayer. Despite the systematic uncertainties introduced by the injection method, injection of Tf under a lipid film results in a slight loss of surface area, indicating loss of film material compared to PBPS only. Conversely, injection of Tf-AuINT results in a significant surface area increase, indicating a larger amount of film material at the air-water surface compared to PBPS only. We attribute the increased surface area upon injection of Tf-AuINT to intercalation into the lipid monolayer due to the increased surface activity of the protein-AuNCs construct, as has been reported for similar constructs based on alpha-lactalbumin interacting with PBPS.[15]

As Tf only did not reveal any measurable surface activity, the apparent loss of film material when injecting Tf under the PBPS monolayer is likely due to bulk interactions between Tf and dissolved lipids. Binding of PBPS molecules to Tf shifts the equilibrium between monolayer-bound and dissolved lipids, leading to further loss of film material.

Atomic force microscopy was further employed to visualize morphological changes in lipid film upon introduction of Tf and Tf-AuINT. Figure 5a shows a monolayer of pure anionic PBPS lipid uniformly deposited onto gold surface via the Langmuir-Schaefer method in contrast to bare gold sputtered surface as shown in Figure 5b, confirming the monolayer deposition of lipid molecules. The lipid film is made from the assembly of small regions with average height and width ~1.7 nm and ~16 nm respectively, as displayed in Figures 5c and d. Inserting Tf and Tf-AuINT underneath the lipid film held at 10 mN/m causes a perturbation in the film where the lipid regions are severely collapsed (Figure 5e, f). AFM results reveal a large extent of disruption in the case of Tf-AuINT, with no discernible packing of lipid regions and only collapsed film with gold nanoclusters with a wide size distribution. Therefore, Tf-AuINT has a high propensity to intercalate into the negatively charged lipid film as compared to Tf only. This is also in agreement with a recent study of alpha-lactalbumin protected gold nanoclusters.[15]

Cell viability studies

Three different cell types were chosen to assess the interaction with Tf-AuINT. Two human cancerous cell lines, ovarian cancer cells (OCCs) and brain cancer cells (glioblastoma-astrocytoma cells), and non-cancerous cells (olfactory ensheating cells, OECs) were incubated with three different concentrations of Tf and Tf-AuINT and the viability was assessed with a LIVE/DEAD assay. For all cell types, there was no increased cell death after incubation with Tf-AuINT or Tf, compared to the blank. One of the dyes in the LIVE/DEAD assay, ethidium homodimer, chelates with DNA and emits red light when excited at 430nm. The dye can only move through compromised cell membranes, and will therefore stain dead cells red. A typical dead cell is shown in figure 6e. Live cells express calcein AM (λ_{ex}=495, λ_{em}=515), as they have esterases that cleave calcein AM to a green fluorescent molecule. Live cells therefore typically have an even intracellular distribution of green fluorescent dye, as can be seen in figure 6f. However, for the OECs cell culture, incubation with Tf-AuINT results in partial colocalization of the calcein – and EthD1-derived fluorescence. This might indicate that Tf-AuINT is associated with the cell membrane, blocking the entry of Ethidium homodimer and calcein, or that there is some photophysical interaction between the Tf-AuINT and the dyes. If the latter were to be the case though, similar observations should have also been made for the glioblastoma-astrocytoma as well as for the OCCs. In the absence of such evidence, and given that Tf-AuINT showed a strong tendency towards the monolayer surface (Figure 4), we attribute the colocalisation of the dyes to an enhanced Tf-AuINT affinity

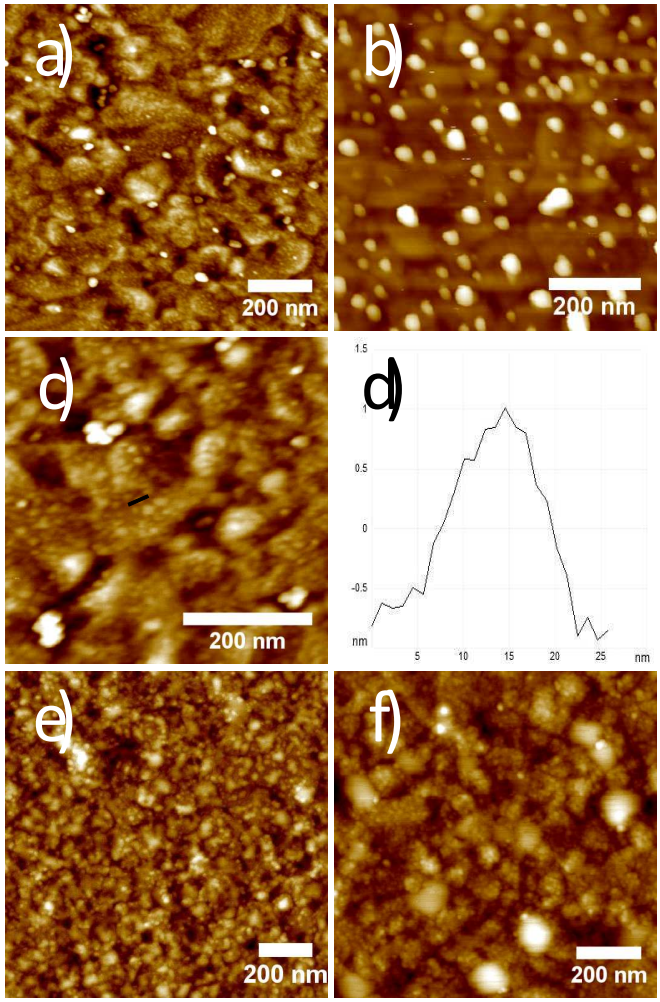

Figure 5: AFM topographical images of lipid films deposited by the Langmuir-Schaefer method at 10 mN/m onto gold sputtered glass substrates. a) Pure PBPS lipid film showing uniform deposition. **b)** Gold sputtered surface prior to lipid deposition. **c)** High resolution view of lipid film and **d)** section analysis of lipid regions. **e)** Disruption in the PBPS lipid film caused by insertion of Tf protein and **f)** Tf protein modified gold nanocluster.

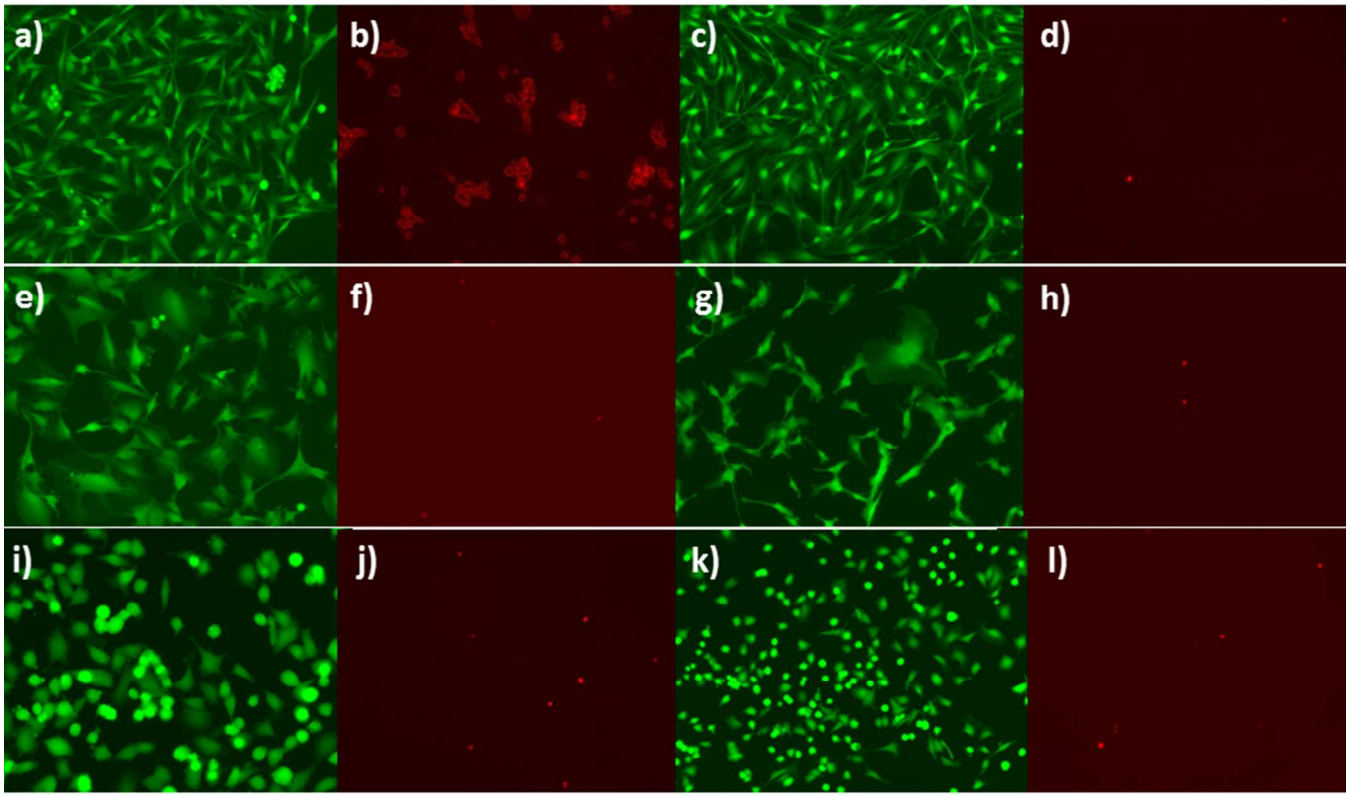

Figure 6: Colocalization of dyes at the membranes of OECs. All cells were incubated for four hours with different concentrations of Tf (1µg/mL, 100µg/mL and 1mg/mL) and Tf-AuINT (1µg/mL, 100µg/mL and 1mg/mL) before staining with LIVE/DEAD assay. **a)** Live and **b)** dead OECs with 1µg/mL Tf-AuINT, control **c)** live and **d)** dead OECs. Glioblastoma cells are imaged from e)-h), with e) and f) displaying cells after incubation of 1mg/mL Tf-AuINT, and g) and h) show the control. Images **i)-l)** show **i)** live and **j)** dead OCCs after incubation of 1mg/mL Tf-AuINT, and the control **k)** live and **l)** dead cells.

with the OEC membrane (Figure 6b). However, unlike OECs, glioblastoma-astrocytoma and OCCs did not exhibit colocalisation of calcein with EthD-1 after incubation with Tf-AuINT (Figure 6, e-f and i-j). Assuming that colocalisation of the dyes may indeed be attributed to enhanced Tf-AuINT affinity towards the cell membrane, the different interactions of the Tf-AuINT with the different cell types may be attributed to intercellular membrane differences between glioblastoma and astrocytoma[30,31], as well as OCC-cells and OECs**.**

Conclusions

We have synthesized Tf-stabilized gold nanostructures using two synthesis routes – with and without the aid of an extrinsic reducing agent ($NaBH_4$). From our results, we can conclude that the amount of AuNPs synthesized strongly depend wether or not $NaBH_4$ is added, and that the concentration of TCAA is important (TfAuXL). Not just the size of the AuNCs and AuNPs seem to be affected by the TCAA concentration and reducing agent, but also the solution stability of Tf-Au constructs appear to be affected. There is a delicate balance between the reducing agent aiding nanostructure formation and causing irreversible unfolding of the polypeptide chain. However, it seems as though a slight unfolding of the protein backbone is favourable for membrane interactions, as Langmuir experiments and AFM clearly show that Tf-AuINT has a greater tendency to interact with biological films, compared to Tf alone. These findings are in agreement with previously published results.[15,18,19] *In vitro* membrane interaction studies on three different cell types indicate that Tf-AuINT might have a different affinity towards different cell types.

Acknowledgements

The authors acknowledge the Department of Chemical Engineering, NTNU, for financial support. Acknowledgements are also given to Moreland *et al*[32]. and Xu *et al*[33]for providing the necessary software (Protein Workshop 4.2.0) for preparation of 3D imaging of Tf. Gurvinder Singh thanks NTNU Nanolab for providing instrumentation facilities. The Research Council

of Norway is acknowledged for the support to the Norwegian Micro-and Nano-Fabrication Facility, NorFab (197411/V30).

Abbreviations

Tf= Transferrin

TCAA= Tetrachloroauric acid

Tf-AuINT= Transferrin stabilized gold prepared via the Intrinsic protocl.

TfAuXL= Transferrin stabilized gold prepared with low concentration of TCAA, via the Extrinsic protocl.

TfAuXH= Transferrin stabilized gold prepared with high concentration of TCAA, via the Extrinsic protocl.

Tf-RED= Transferrin incubated with $NaBH_4$

AuNCs= Gold nanoclusters

AuNPs= Gold nanoparticles

Trp= Tryptophan

(1) Deheer, W. A. *Rev. Mod. Phys.* **1993**, *65*, 611.

(2) Zheng, J.; Nicovich, P. R.; Dickson, R. M. In *Annual Review of Physical Chemistry*; Annual Reviews: Palo Alto, 2007; Vol. 58, p 409.

(3) Xie, J. P.; Zheng, Y. G.; Ying, J. Y. *J. Am. Chem. Soc.* **2009**, *131*, 888.

(4) Chen, H. Y.; Li, B. W.; Ren, X. Y.; Li, S. N.; Ma, Y. X.; Cui, S. S.; Gu, Y. Q. *Biomaterials* **2012**, *33*, 8461.

(5) Le Guevel, X.; Daum, N.; Schneider, M. *Nanotechnology* **2011**, *22*, 7.

(6) Retnakumari, A.; Jayasimhan, J.; Chandran, P.; Menon, D.; Nair, S.; Mony, U.; Koyakutty, M. *Nanotechnology* **2011**, *22*, 11.

(7) Shiang, Y. C.; Huang, C. C.; Chen, W. Y.; Chen, P. C.; Chang, H. T. *J. Mater. Chem.* **2012**, *22*, 12972.

(8) Sun, C. J.; Yang, H.; Yuan, Y.; Tian, X.; Wang, L. M.; Guo, Y.; Xu, L.; Lei, J. L.; Gao, N.; Anderson, G. J.; Liang, X. J.; Chen, C. Y.; Zhao, Y. L.; Nie, G. J. *J. Am. Chem. Soc.* **2011**, *133*, 8617.

(9) Chen, T. H.; Tseng, W. L. *Small* **2012**, *8*, 1912.

(10) Hu, L. Z.; Han, S.; Parveen, S.; Yuan, Y. L.; Zhang, L.; Xu, G. B. *Biosens. Bioelectron.* **2012**, *32*, 297.

(11) Wang, X. X.; Wu, Q.; Shan, Z.; Huang, Q. M. *Biosens. Bioelectron.* **2011**, *26*, 3614.

(12) Wen, F.; Dong, Y. H.; Feng, L.; Wang, S.; Zhang, S. C.; Zhang, X. R. *Anal. Chem.* **2011**, *83*, 1193.

(13) Le Guével, X.; Hötzer, B.; Jung, G.; Hollemeyer, K.; Trouillet, V.; Schneider, M. *Journal of Physical Chemistry C* **2011**, *115*, 10955.

(14) Retnakumari, A.; Setua, S.; Menon, D.; Ravindran, P.; Muhammed, H.; Pradeep, T.; Nair, S.; Koyakutty, M. *Nanotechnology* **2010**, *21*.

(15) Lystvet, S. M.; Volden, S.; Singh, G.; Rundgren, I. M.; Wen, H.; Halskau, O.; Glomm, W. R. *The Journal of Physical Chemistry C* **2013**, *117*, 2230.

(16) Lystvet, S. M.; Volden, S.; Singh, G.; Yasuda, M.; Halskau, O.; Glomm, W. R. *RSC Advances* **2013**, *3*, 482.

(17) Volden, S.; Lystvet, S. M.; Halskau, O.; Glomm, W. R. *RSC Adv.* **2012**, *2*, 11704.

(18) Lystvet, S. M.; Volden, S.; Halskau, O.; Glomm, W. R. *Soft Matter* **2011**, *7*, 11501.

(19) Lystvet, S. M.; Volden, S.; Yasuda, M.; Halskau, O.; Glomm, W. R. *Nanoscale* **2011**, *3*, 1788.

(20) Gomme, P. T.; McCann, K. B. *Drug Discov. Today* **2005**, *10*, 267.
(21) Qian, Z. M.; Li, H. Y.; Sun, H. Z.; Ho, K. *Pharmacol. Rev.* **2002**, *54*, 561.
(22) Yersin, A.; Osada, T.; Ikai, A. *Biophys. J.* **2008**, *94*, 230.
(23) Chan, W. C. W.; Nie, S. M. *Science* **1998**, *281*, 2016.
(24) Anabousi, S.; Bakowsky, U.; Schneider, M.; Huwer, H.; Lehr, C. M.; Ehrhardt, C. *Eur. J. Pharm. Sci.* **2006**, *29*, 367.
(25) Yang, P. H.; Sun, X. S.; Chiu, J. F.; Sun, H. Z.; He, Q. Y. *Bioconjugate Chem.* **2005**, *16*, 494.
(26) Glomm, W. R.; Volden, S.; Halskau Jr, Ø.; Ese, M. H. G. *Analytical Chemistry* **2009**, *81*, 3042.
(27) Glomm, W. R.; Halskau Jr, Ø.; Hanneseth, A. M. D.; Volden, S. *Journal of Physical Chemistry B* **2007**, *111*, 14329.
(28) Lakowicz, J. R. *Principles of Fluorescence Spectroscopy*; Springer: New York, 2006.
(29) Glomm, W. R.; Volden, S.; Halskau, O.; Ese, M. H. G. *Anaytical Chemistry.* **2009**, *81*, 3042.
(30) He, H.; Conrad, C. A.; Nilsson, C. L.; Ji, Y.; Schaub, T. M.; Marshall, A. G.; Emmett, M. R. *Analytical Chemistry* **2007**, *79*, 8423.
(31) Yates, A. J.; Thompson, D. K.; Boesel, C. P.; Albrightson, C.; Hart, R. W. *Journal of Lipid Research* **1979**, *20*, 428.
(32) Moreland, J. L.; Gramada, A.; Buzko, O. V.; Zhang, Q.; Bourne, P. E. *BMC Bioinformatics* **2005**, *6*.
(33) Xu, D.; Zhang, Y. *PLoS ONE* **2009**, *4*.